Preliminary Results on Dynamic Analysis of a New Test Rig for Wheel-Rail Contact Studies

Meysam Naeimi[1*], Zili Li[2], Rolf Dollevoet[3]
[1,2,3]Section of Railway Engineering, Faculty of Civil Engineering and Geoscience, Delft University of Technology, Delft, the Netherlands

ARTICLE INFO	ABSTRACT
	A new reduced–scale test rig is developed owing to significantly contribute to the applicability of the laboratory tests on rolling contact fatigue (RCF) in wheel-rail material. This paper introduces the dynamic analysis of the test rig, in order to assess the vibration behaviour of the system with respect to contact phenomenon. Finite element modelling (FEM) is used to simulate the mechanical behaviour of the test rig, representing dynamic response of the components under wheel impact loading conditions. To study the influence of scaling on the new rig, and to understand the functional relationships between the mechanical parameters, two tentative scales i.e. 1/5 and 1/7 are defined as global scale factors of the rig. FE models of the scaled test rig together with a model of actual-size railway system are analysed and their dynamic characteristics are compared. Based on results of dynamic simulations, a strong evidence of association between the chosen scale factors and dominant frequencies of vibrations was found. The major dynamic parameters of the new test rig are lastly derived based on the numerical investigations.

1. Introduction

A considerable amount of literature has been published to advance the understanding of the influence of loading conditions on rolling contact fatigue (RCF) damage development in rail material; among them, numerous studies, for example [1-5], attempted to explain the rail RCF problem using a wide range of numerical methods and computational approaches. These works, carried out based on principles of the contact mechanics and fracture mechanics, described the contact behaviour and damage development of the wheel and rail materials. During the past three decades, a significant number of works has also become available on

experimental investigation of the wheel–rail RCF with either full or reduced scale strategies. Researchers have carried out experiments almost from the beginning of contact mechanics research in railway field and various test rigs have been introduced until present.

Full–scale test rigs are useful tools for assessing dynamic characteristics of the vehicle–track system when their high costs are justified by their particular use. Where the area of research is rather broader, and the behaviour of a particular prototype vehicle is not the primary area of interest, then the use of a scaled test rig can offer a number of advantages in experimental studies [6, 7]. The most obvious of these advantages is, of course, the less space

occupied by the scaled rigs; this is coupled to a large cost saving and an ease of operability. A scaled rig is much easier to maintain and the mechanical handling of the testing facility is more manageable. That is also far easier to investigate different parameters, modify the testing conditions and run long-term duration experiments.

In order to enhance the insight in the relationships among loading conditions, microstructural features, properties of the rail material and resulting RCF damage, a new reduced–scale test rig is developed. Experiments on this rig mainly aim at improving the predictability of RCF damage development in rails. The rig is capable of assessing damage development phases under laboratory-controlled conditions, and of predicting the effects of material microstructure on the defect initiation and growth. The test facility consists of several wheel components each of them rotating around a central pivot and running at a ring–shape rail track. A schematic view of the wheel-track system in the test rig is given in Figure 1. Wheel assemblies are composed of several subassemblies representative for primary suspensions of the railway vehicle and are supported by the top frame structure. It is possible to activate multiple wheels up to four in the system, moving on the track simultaneously. The rail track assembly is composed of different subassemblies likewise the components of actual track structure. The top surface of the horizontal rail ring is the running band in contact with the wheel tread.

Although an extensive research has been carried out on experimental aspects of the RCF problem in rail, see some examples in [8-11], dynamic characteristics of the testing facilities did not receive enough attention until present. Most of the works in the technical literature dedicated to the results of experiments obtained from the test rigs, while less attention paid on dynamic behaviour of the rigs. This means, though researchers carried out different tests on railway rigs, less attention was paid to the dynamic nature of the test rigs, particularly when the rigs were designed or developed. This paper as part of undergoing researches related to design of the prescribed rig, examines the dynamic behaviour of the test facility. The main purpose of this study is to develop an understanding of the effects of different scale factors on the dynamics of the system. Several numerical models are introduced based on finite element method (FEM), to describe the vibration behaviour of the new rig with different scales. The influence of chosen scale strategies on dynamic responses are assessed.

2. Scaling law

Various scaling strategies are available for reduced-scale mechanisms. The starting point to define similarity in testing mechanisms, is the geometric scaling, i.e. the definition of scaling factors for all dimensions in the test rig. General scaling rules can be used to relate small-scale rigs to their full size equivalents. References [12-16] are some examples of available studies on scaling methodologies in railway test facilities. Most of these works are based on reducing all dimensions by the scale factor N, whereas material properties are kept the same [12]. The scaling strategy of [12, 16] is used in the present research to derives parameters of the new test rig, based on scaling are kept the same [12]. The scaling strategy of [12, 16] is used in the present research to derives factors on original variables. Table 1 gives the scaling factors of test rig parameters (such as dimension, mass, stiffness, damping and material properties), obtained using the chosen similarity law; see [17, 18] for details of scaling strategies.

According to the scale factors in Table 1, one can see that the overall scale factor of the rig (parameter N) has significant influence on all variables. This means, the geometric and mechanical properties of the system are directly dependent upon the overall scale. To simulate the test rig behaviour, two tentative scales i.e. N=5 and N=7 were selected as the overall 3 scale of the new rig and all corresponding variables were determined based on the scale factors in Table 1. By applying the prescribed values of N, results of dimensional analysis on the equivalent one–fifth and one–seventh scaled rigs are determined as listed in Table 2. The values of the actual vehicle–track system in this table are taken from [19, 20], for the wheel

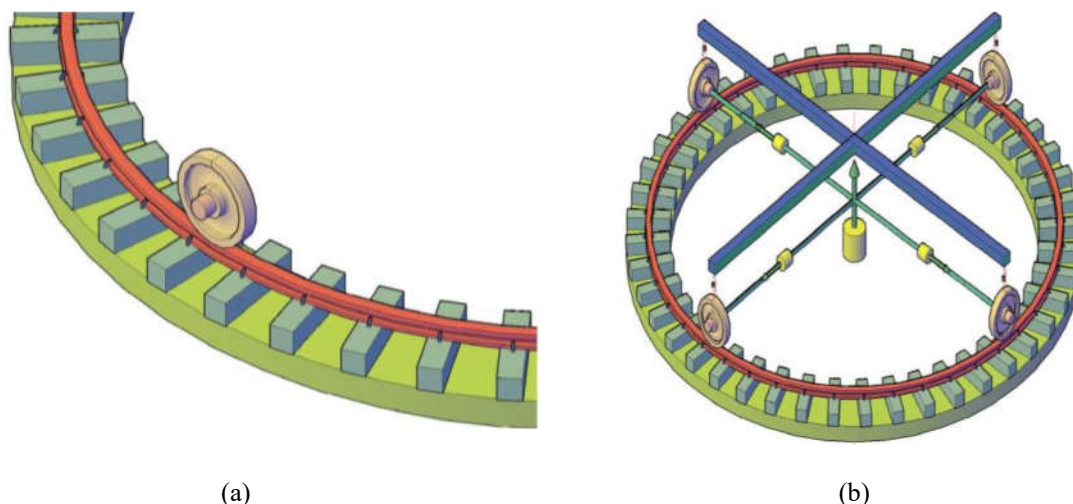(a)   (b)

Figure 1. A schematic view of the wheel-track system in the test rig (single/multiple wheels over half of a rail track)

Table 1: The similarity law of the small-scale test rig

Variable/ parameter	Variable notation	Units	Scale notation	Scale factors
Distance	L	m	ϕ_L	$1/N$
Cross section	A	m^2	ϕ_A	$1/N^2$
Volume	$Vol.$	m^3	ϕ_{Vol}	$1/N^3$
Moment of inertia	I	m^4	ϕ_I	$1/N^4$
Density	ρ	$kg/m3$	ϕ_ρ	1
Mass	M	kg	ϕ_M	$1/N^3$
Young's modulus	e	N/m^2	ϕ_E	1
Poisson's ratio	v	$None$	ϕ_v	1
Force	F	N	ϕ_F	$1/N^2$
Moment	T	Nm	ϕ_T	$1/N^3$
Stress	σ	N/m^2	ϕ_σ	1
Strain	ε	$None$	ϕ_ε	1
Stiffness	K	N/m	ϕ_K	$1/N$
Damping	C	$N.s/m$	ϕ_C	$1/N^2$
Frequency	f	Hz	ϕ_f	N
Time	t	s	ϕ_t	$1/N$
Velocity	V	m/s	ϕ_V	1
Acceleration	a	m/s^2	ϕ_a	N
Friction coefficient	μ	$None$	ϕ_μ	1

profile S1002, rail profile UIC54E1 and concrete sleepers. Corresponding values of parameters for the scaled cases were calculated by applying scale factors on original quantities.

By applying the mentioned scale factors over wheel–track components, the scaled geometry of the test rig components were determined. The precise target values of the geometric parameters in the reduced scale conditions are demonstrated in Figure 2. Dynamic simulations in the current study performed for the precise geometries of 1/5 and 1/7 models.

From engineering viewpoints, it is not possible to exactly employ the calculated

geometries (nominal values) and variables of Table 2 and Figure 2 in the scaled cases. Indeed, nominal values need to be further adjusted in the construction stage of the rig, owing to reach practical parameters for convenient manufacturing.

3. Dynamic simulation of the test

Finite element method (FEM) is widely used in wheel–rail contact problem. In most of previous works, two solid rolling bodies are put together to generate an elliptic contact and simulate rolling condition. With the finite element method the half–space assumption can easily be dropped, and the nonlinear material properties can be well considered [19].

Furthermore, it can deal with the dynamic issues in contact problem by performing transient FE simulations. The wheel–track interaction was treated in [19, 20] with an explicit FE method. In the current research, the same FE approach is used for the reduced–scale prototypes. The hybrid multi–body–finite–element model of half–track and one wheel, shown in Figure 3, is created to simulate the dynamic behaviour of the wheel–track system.

Table 2: Mechanical parameters for the actual system and the equivalent scaled rigs

| Mechanical variables (unit)	Actual condition	1/5 scaled rig	1/7 scaled rig
Rail weight per length (Kg/m)	54.42	2.18	1.11
Sleeper mass M_s (kg)	200	1.60	0.58
Stiffness of primary suspension, K_c (kN/m)	1150	230	164
Damping of primary suspension, C_c ($N.s/m$)	2500	100	51
Stiffness of rail pad, K_p (kN/m)	1300000	260000	185714
Damping of rail pad, C_p ($N.s/m$)	45000	1800	918
Stiffness of ballast, K_b (kN/m)	45000	9000	6429
Damping of ballast, C_b ($N.s/m$)	32000	1280	653
Young's modulus of wheel–rail material, E_r (GP)	210	210	210
Poisson's ratio of wheel–rail material, v_r	0.3	0.3	0.3
Density of wheel–rail material, ρ_r ($kg/m3$)	7800	7800	7800
Young's modulus of concrete material, E_c (GP)	38	38	38
Poisson's ratio of concrete sleeper material, v_c	0.2	0.2	0.2
Density of sleeper material, ρ_c ($kg/m3$)	2500	2500	2500
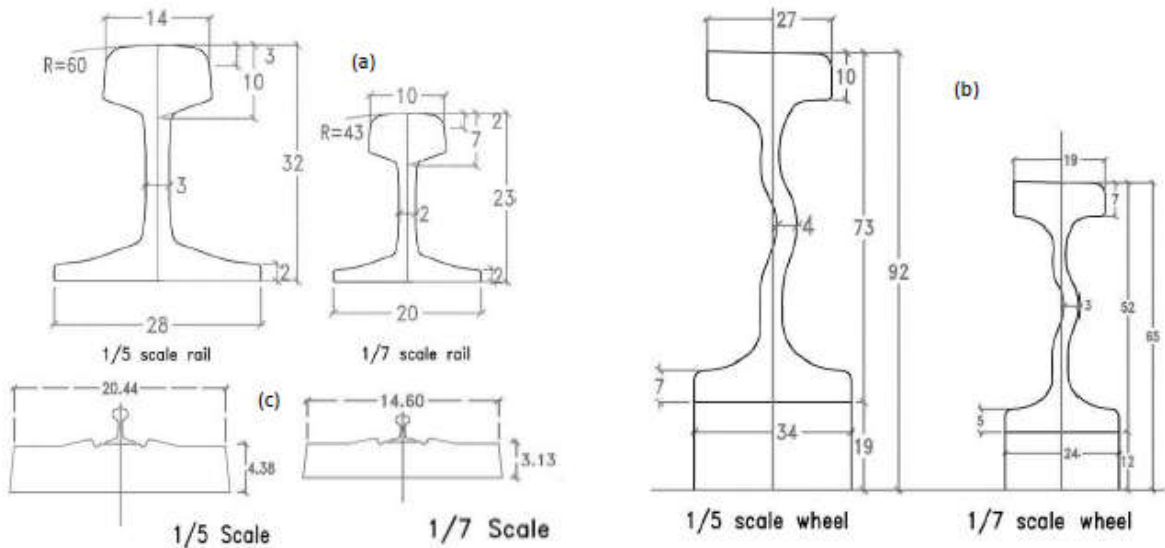
Figure 2. The Geometry of components in 1/5 and 1/7 scaled test rig, all dimensions in mm, (a) rails, (b) wheels, (c) sleepers

The FE models of the scaled test rig were built based on two scale scenarios (1/5 and 1/7) according to the proposed geometries of Figure 2. Besides the scaled models, the actual-size model of wheel–track system was also modelled for the purpose of comparison.

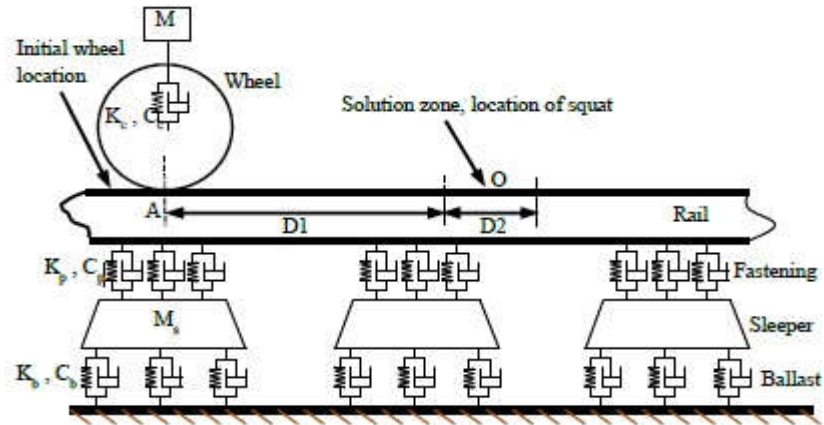Three-dimensional FE analysis with explicit

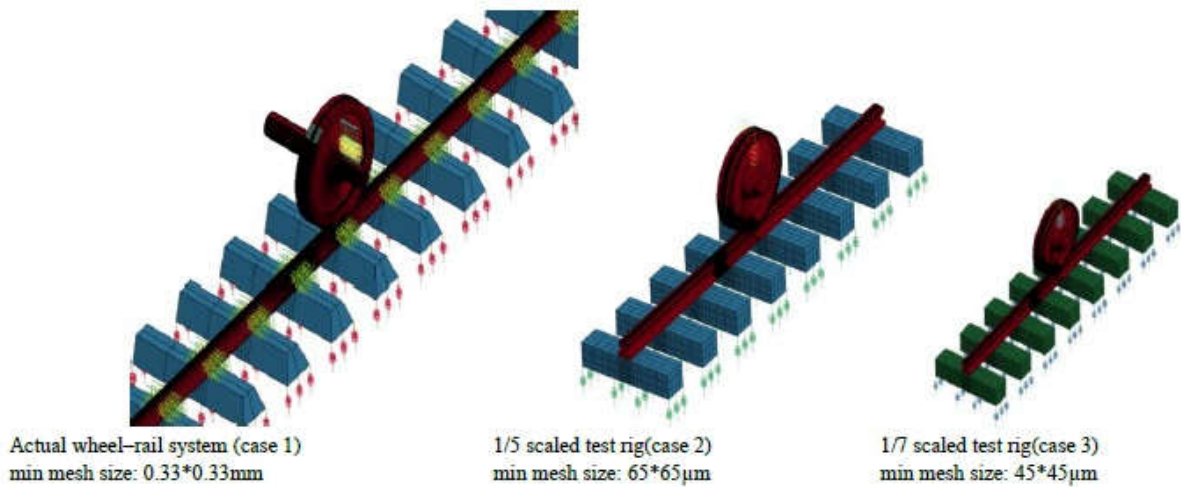Figure 3. The hybrid model of a single wheel on a half rail track system

Actual wheel–rail system (case 1)
min mesh size: 0.33*0.33mm

1/5 scaled test rig(case 2)
min mesh size: 65*65μm

1/7 scaled test rig(case 3)
min mesh size: 45*45μm

Figure 4. FE modelling of the wheel–track dynamic interaction in various scenarios

Table 3. Assumed parameters for dynamic simulations

| Simulation assumptions	Actual condition	1/5 scaled rig	1/7 scaled rig
Lumped sprung mass, static load M_c (kg)	12000	480	245
Wheel weight, unsprung mass (kg)	900	7.20	2.62
Rolling speed (km/h)	60	60	60
Wheel angular speed (rpm)	13.46	67.28	94.19
Wheel angular speed (Rad/s)	84.74	423.70	593.17
Traveling length on rail, D1+D2 (mm)	1000	200	142
Entire traveling time for wheel, t_{max} (ms)	42	8	6
Friction coefficient	0.3	0.3	0.3
Traction coefficient	0.15	0.15	0.15
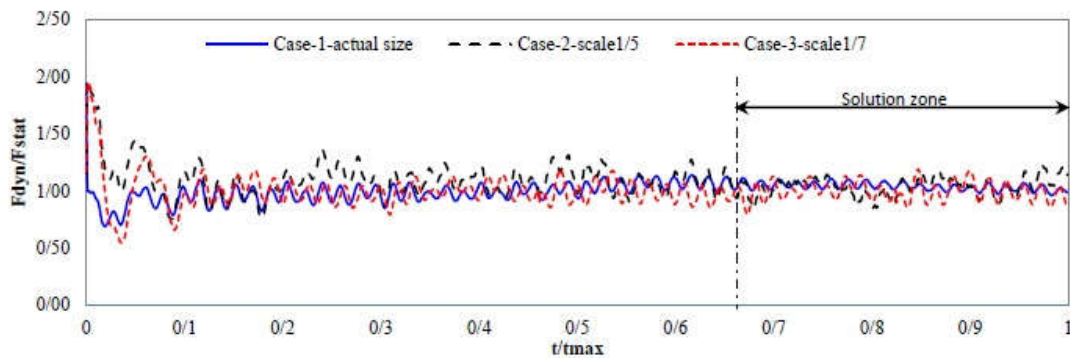
Figure 5. Comparative results of vertical wheel–rail contact forces for the smooth rail in three FE models
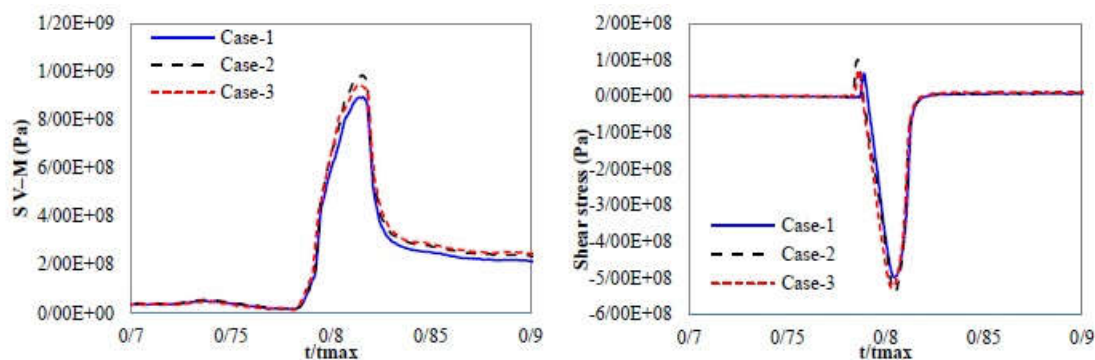

Figure 6. Distribution of nodal stress in different FE models, Von Mises stress (left), shear stress (right)

algorithm was employed and particular attention was paid to the contact zone, so that a sufficient accuracy was obtained by applying finest mesh arrangement in the contact zone.

The FE models of the discussed alternatives i.e. the actual-size, 1/5 scale and 1/7 scale models are shown in Figure 4. The smallest element size at the investigated zones of each FE model is shown below the models. Since the analogical models were made up of the same materials, vibration behaviours of the scaled models were maintained in similarity of the actual-size model. elements. Mechanical parameters and material properties were set in the models based on the values in Table 2.

Nonlinear contact took place on the level of surface between the scaled wheel and rail Table 3 gives the assumptions of dynamic simulations in various models. Based on this table, an average rolling speed of 60 km/h was considered

for all scenarios as an operational speed practically conceivable in the test rig. A combination of vertical and tangential loads was applied in dynamic simulations. The vertical sprung mass on wheel component was assumed 12000, 480 and 245 kg for the case 1, 2 and 3 correspondingly (see Table 3). The dead weights of the wheel–rail components were automatically included in the numerical analysis. A traction coefficient (ratio of tangential to vertical load) of 0.15 was applied in all models. Frictional rolling contact problem was treated in all cases by assuming a constant friction coefficient between the wheel and rail material.

4. Results and discussions

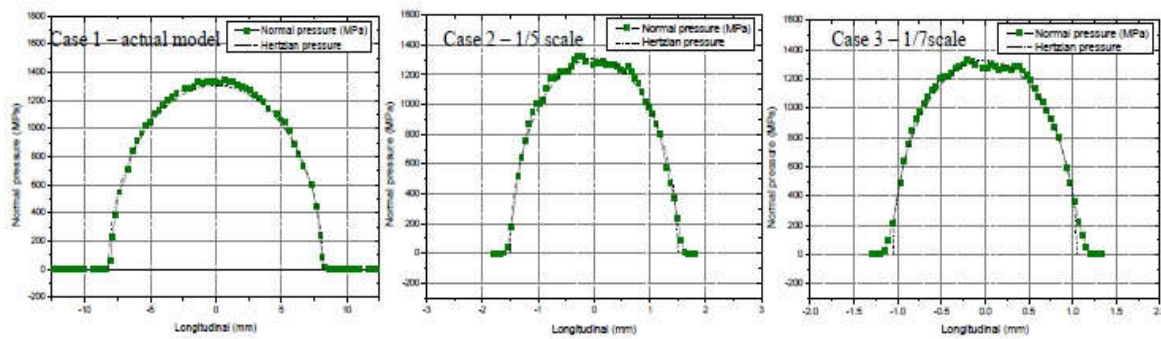### 4.1. Wheel-rail contact forces

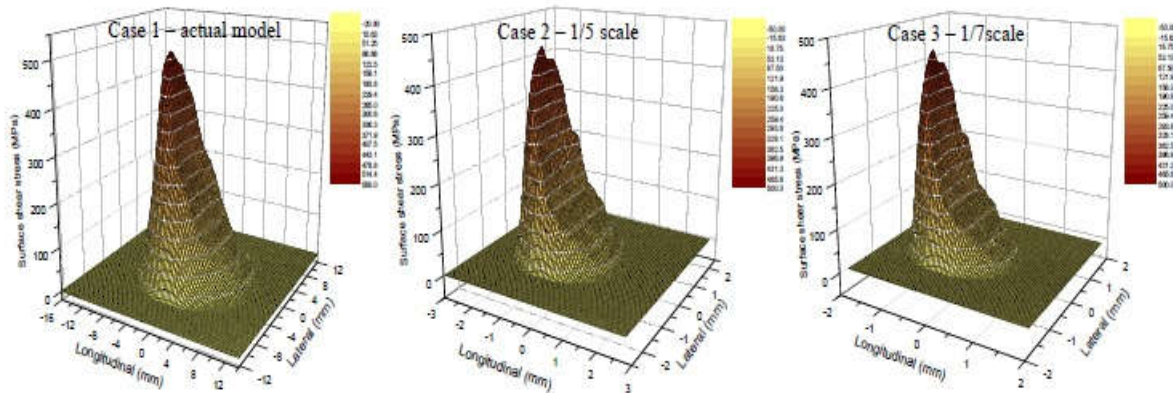Figure 7. Distributions of pressure in contact patches of three models

Figure 8. Distributions of surface shear stress in contact patches of three models

After the rolling initialization with a constant velocity, the dynamic simulation was started. Meanwhile, the required loads applied on wheel let it to simulate frictional rolling condition in the presence of normal and tangential loads. Dynamic forces in each FE model were obtained during the entire wheel passage. The results of the wheel–rail contact forces in three FE models were extracted as demonstrated in Figure 5. In order to display results of different models in this figure, the time axes were normalised by dividing the values over their peak quantities (simulation time). Moreover, the force vectors were normalised relative to the corresponding static loads (for the purpose of comparison). Hence, a value of the dynamic force greater than one represents a load increase with respect to the static wheel load. As shown in this figure, contact forces in all cases have some fluctuations around the static values. High frequency vibrations and wave propagations in the wheel and rail continua mainly caused these fluctuations. Due to higher accuracy in the solution zone, fluctuations were decreased in this part with fair attenuation rates. Although contact forces were quite different in various FE models, dynamic implication factors (F_{dyn}/F_{stat}) were relatively in the same range.

4.2. Contact patch stresses

To evaluate the distribution of stresses in the contact patches of different FE models, further simulations were carried out using FE models with higher accuracy. The size of elements in the contact zones reduced to a third of the previous
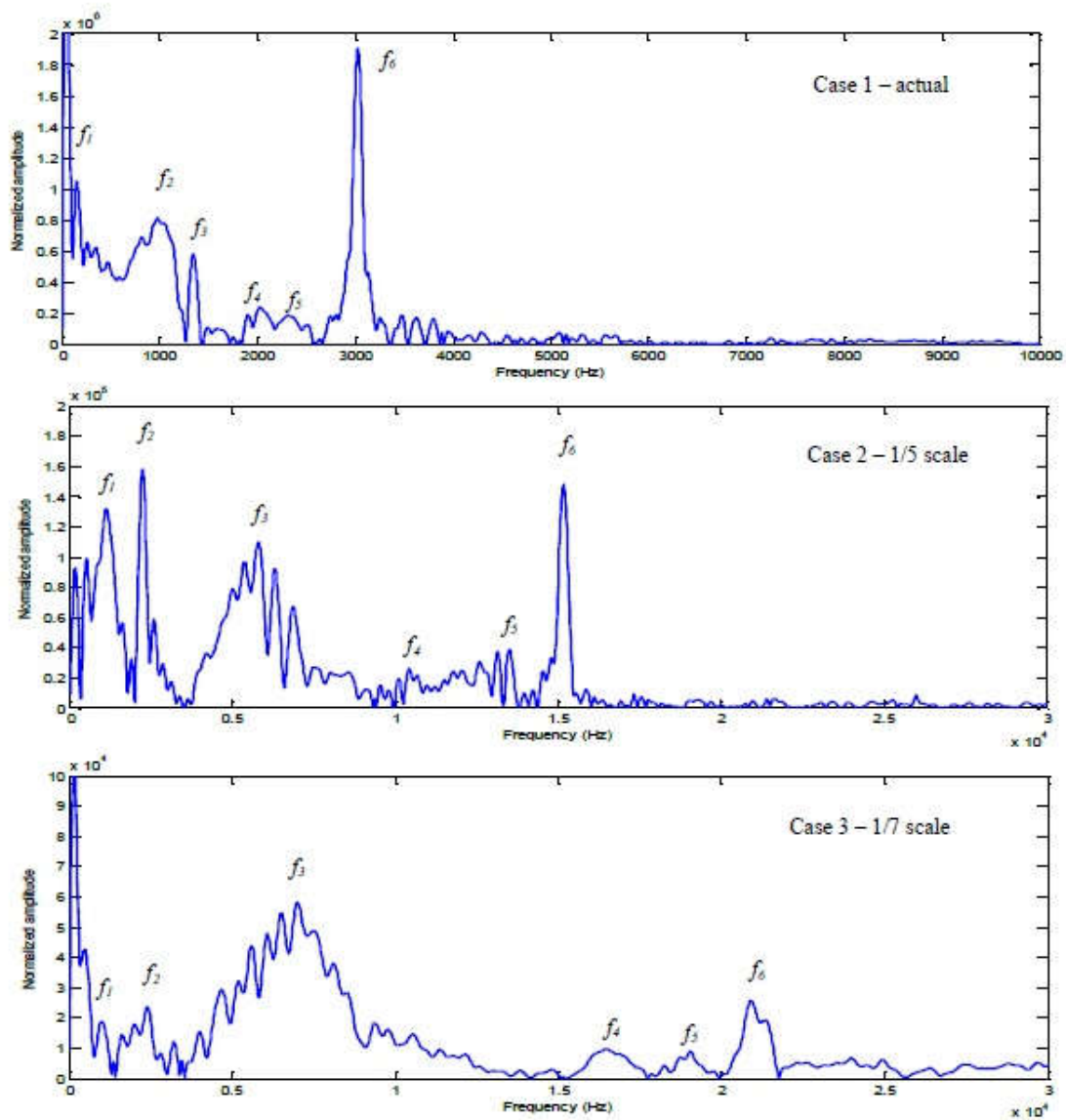
Figure 9. The amplitude spectra of the wheel–rail dynamic forces in different FE models

Table 4. Dominant frequency contents in all amplitude spectra of the dynamic forces in smooth rail models

Dominant frequency No.	FREQ– Case1–actual	FREQ–1/5 scale	FREQ–1/7 scale	Ratio–1/5 scale	Ratio–1/7 scale
f1	158	1108	986	7.01	6.24
f2	966	2250	2441	2.33	2.53
f3	1333	5789	6996	4.34	5.25
f4	2026	10440	16410	5.15	8.10
f5	2333	13150	19060	5.64	8.17
f6	3032	15170	20920	5.00	6.90
Average ratio (except f1 and f2 values)				5.03	7.10

models. Figure 8 and 9 show the distributions of pressure and surface shear stress in contact patches of three models. According to these results, further evidences for approximate stress levels in different modes were observed. In contrast, contact patch sizes and dimensions were far smaller in the scaled models than the actual system. The reduction rates were according to the same scale factors that applied on geometries (Table 1).

4.3. Frequency responses

Performing a fast Fourier transform (FFT) analysis, dynamic wheel–rail forces were transformed to the frequency domain and the results in different FE models were compared. The amplitude spectra of dynamic forces are shown in Figure 9. To compare frequency contents of the forces in various models, locations of the dominant frequencies (with peak amplitudes) marked as $f1$ to $f6$ in each diagram. A wide range of frequencies starting from zero to 30 kHz was considered owing to cover all low frequency and high frequency contents, particularly for the scaled cases.

The magnitudes of dominant frequencies in all curves were determined and the results were summarized in Table 4. This table compares frequencies of the vibration in three FE models. To identify the relationships between dominant frequencies, ratios of frequencies relative to the actual case are also given in the table.

From the data in Table 4, it is apparent that there is a significant difference between average frequencies of the models. Comparing the results, an evidence of linear scaling on frequency values were distinguished. Apart from two first dominant frequencies $f1$ and $f2$, the rest of frequencies in the scaled models had near ratios relative the actual case. The average ratios of the dominant frequencies in the 1/5 and 1/7 scaled models were 5.03 and 7.10 relative to the actual case, respectively. Note that $f1$ and $f2$ results were excluded from average calculations as outliers. Obtained ratios were fairly close to the overall scale factors of the test rig in two scaled scenarios (N=5 and N=7). This finding confirms the anticipated association between the

scale factor and the frequency parameter and supports the previous expectation of linear scale on frequency in Table 1 ($\phi f=N$).

5. Conclusions

A new reduced–scale test rig consisting of rotating wheel components on a ring–shape rail track system was developed for wheel-rail contact studies. Applying the scaling law, geometries and mechanical properties of the small-scale test rig was determined. Using finite element method, the transient dynamic behavior of the test rig models and the actual railway were studied. Dynamic forces, stress levels, contact patch sizes and frequency contents of dynamic forces in the test rig models compared to the results from the actual railway system. The results of dynamic simulations confirmed predictions of scaling factors on different variables according to the selected scaling law:

1) The stress levels of the wheel-rail material in the test rig environment were relatively identical to the actual railway. This was a significant advantage of the selected scaling strategy, confirmed by the numerical simulations.

2) A linear increase in the frequency contents with the scale factor of N was observed almost for all the transient simulations.

3) The scale factors on dynamic forces were in the order of 1/N2.

4) Reverse-linear scale factors of 1/N were observed on the dimensions of contact patches in different cases.

Taken together, these findings support the effectiveness of the chosen scaling strategy for the test rig in terms of dynamic behaviors and parameters.

References

[1] S. Bogdanski, M. Olzak, J. Stupnicki, Numerical stress analysis of rail rolling contact fatigue cracks. Wear, **191**(1-2), (1996), pp.14-24.

[2] J. Ringsberg, B. Josefson, Finite element analyses of rolling contact fatigue crack initiation in railheads. Proceedings of the Institution of Mechanical Engineers, Part F: Journal of Rail and Rapid Transit, **215**(4), (2001), pp.243-259.

[3] S. Bogdański, M.W. Brown, Modelling the three-dimensional behaviour of shallow rolling contact fatigue cracks in rails. Wear, **253**(1), (2002), pp.17-25.

[4] J. Tillberg, F. Larsson, K. Runesson, A study of multiple crack interaction at rolling contact fatigue loading of rails. Proceedings of the Institution of Mechanical Engineers, Part F: Journal of Rail and Rapid Transit, **223**(4), (2009), pp.319-330.

[5] J. Brouzoulis, M. Ekh, Crack propagation in rails under rolling contact fatigue loading conditions based on material forces. International Journal of Fatigue, **45**, (2012), pp.98-105.

[6] W. Zhang, H. Dai, Z. Shen, J. Zeng, Chapter 14, Roller Rigs, in Handbook of railway vehicle dynamics, S. Iwnicki, Editor. (2006), CRC Press, Boca Raton FL (USA).

[7] P. Allen, Chapter 15, Scale Testing, in Handbook of railway vehicle dynamics S. Iwnicki, Editor. (2006), CRC Press, Boca Raton FL (USA).

[8] D.T. Eadie, D. Elvidge, K. Oldknow, R. Stock, P. Pointner, J. Kalousek, P. Klauser, The effects of top of rail friction modifier on wear and rolling contact fatigue: Full-scale fail-wheel test rig evaluation, analysis and modelling. Wear, **265**(9-10), (2008), pp.1222-1230.

[9] B. Allotta, L. Pugi, M. Malvezzi, F. Bartolini, F. Cangioli, A scaled roller test rig for high-speed vehicles. Vehicle system dynamics, **48**(S1), (2010), pp.3-18.

[10] T.M. Bandula-Heva, M. Dhanasekar, P. Boyd, Experimental investigation of wheel/rail rolling contact at railhead edge. Experimental Mechanics, **53**(6), (2013), pp.943-957.

[11] O. Arias-Cuevas, Z. Li, R. Lewis, E.A. Gallardo-Hernandez, Rolling-sliding laboratory tests of friction modifiers in dry and wet wheel-rail contacts. Wear, **268**(3-4), (2010), pp.543-551.

[12] T. Armstrong, D. Thompson, Use of a reduced scale model for the study of wheel/rail interaction. Proceedings of the Institution of Mechanical Engineers, Part F: Journal of Rail and Rapid Transit, **220**(3), (2006), pp.235-246.

[13] A. Jaschinski, H. Chollet, S.D. Iwnicki, A. Wickens, J. von Wurzen, The application of roller rigs to railway vehicle dynamics. Vehicle System Dynamics, **31**(5-6), (1999), pp.345-392.

[14] J. Koch, N. Vincent, H. Chollet, O. Chiello, Curve squeal of urban rolling stock—Part 2: Parametric study on a 1/4 scale test rig. Journal of sound and vibration, **293**(3), (2006), pp.701-709.

[15] B.G. Eom, B.B. Kang, H.S. Lee, Design of small-scaled derailment simulator for investigating bogie dynamics. International Journal of Railway, **4**(2), (2011), pp.50-55.

[16] C. Heliot, Small-scale test method for railway dynamics. Vehicle System Dynamics, **15**(sup1), (1986), pp.197-207.

[17] M. Naeimi, Z. Li, R. Dollevoet, Scaling strategy of a new experimental rig for wheel-rail contact. International Journal of Mechanical, Aerospace, Industrial and Mechatronics Engineering, **8**(12), (2014), pp.1787-1794.

[18] M. Naeimi, Z. Li, R.H. Petrov, R.P.B.J. Dollevoet, J. Sietsma, J. Wu, Substantial fatigue similarity of a new small-scale test rig to actual wheel-rail system. International Journal of Mechanical, Aerospace, Industrial and Mechatronics Engineering, **8**(12), (2014), pp.1795-1803.

[19] X. Zhao, Z. Li, The solution of frictional wheel–rail rolling contact with a 3D transient finite element model: Validation and error analysis. Wear, **271**(1–2), (2011), pp.444-452.

[20] X. Zhao, Z.L. Li, R. Dollevoet, The vertical and the longitudinal dynamic responses of the vehicle-track system to squat-type short wavelength irregularity. Vehicle System Dynamics, **51**(12), (2013), pp.1918-1937.